Available online at www.sciencedirect.com

ScienceDirect

journal homepage: www.elsevier.com/locate/issn/15375110

Research Paper

Mapping spatially distributed material properties in finite element models of plant tissue using computed tomography

Christopher J. Stubbs [a], *Ryan Larson* [b], *Douglas D. Cook* [b,*]

[a] *Department of Mechanical Engineering, University of Idaho, Moscow, ID, 83844, USA*
[b] *Department of Mechanical Engineering, Brigham Young University, Provo, UT, 84602, USA*

ARTICLE INFO

Article history:
Received 27 April 2020
Received in revised form
9 October 2020
Accepted 15 October 2020

Keywords:
Biomechanics
Computational
Finite element
Maize
Plant
Stalk

Plant tissues are often heterogeneous. To accurately investigate these tissues, methods to spatially map these tissue stiffness values onto finite element models are required. The aim was to study the feasibility of using specimen-specific computed tomography data to inform the spatial mapping of Young's modulus values on finite element models.

Specimen-specific finite element models with mapped elastic moduli values were developed. The validation models predicted the structural response of the specimen tests within 11.0% of the physical test data. The ability of the models to accurately predict the force-displacement response of the specimen in a different test configuration was considered to be positive validation of the mapping approach. The existence of a model with accurate spatial distribution of material stiffnesses allows for investigations into the stress patterns within the rind and pith tissues. Typically, structural failure in transverse compression manifests as a crack that propagates in the pith along the line of load. In building detailed FEM analyses, we are able to investigate in more detail how the stress is distributed through the pith, and further investigate the causes of the stress concentrations that ultimately lead to the structural failure of the specimen.

A method was developed for determining the relationship between computed-tomography intensity and the transverse elastic modulus in maize stalks. The mapping was used to accurately predict the response of each specimen thus indicating that the mapping relationship is appropriate for modelling and stress analysis activities.

1. Introduction

Biological materials typically exhibit spatial variation of mechanical properties (Gourion-Arsiqaud et al., 2009; Manjubala et al., 2009; Wimmer et al., 1997). In some scenarios mechanical properties can be measured directly, such as with nano-indentation (Cuy et al., 2002; Wimmer et al., 1997; Zysset et al., 1999). In others, these properties co-vary with other physical measurements of the material. When these covariance patterns are known, estimates of one property can be obtained from measurements of a different property. This

* *Corresponding author.*
E-mail address: Ddc971@byu.edu (D.D. Cook).

https://doi.org/10.1016/j.biosystemseng.2020.10.008

technique has been used in human and animal tissue biomechanics, such as estimating the Young's modulus of a material based on its second harmonic autofluorescence (Liu et al., 2019).

Cellular materials such as plant tissues often show a linear relationship between the mechanical properties of the material and the density of the material (Gibson, 2005), and the intensity of X-ray computed tomography (CT) data correlates with material density (Teo et al., 2006; Zhang et al., 2010). This suggests that CT intensity could be used to infer the distribution of mechanical tissue properties (Kaneko et al. 2003, 2004; Snyder and Schneider, 1991). This approach has been successfully employed to model the heterogeneity of bone (Hammond et al., 2018; Helgason et al., 2008), where a linear relationship between CT intensity and mechanical properties of human bone provides accurate results (Ciarelli et al., 1991; McBroom et al., 1985; Rho et al., 1995). These relationships have been used to create finite element models using a variety of CT-informed material mapping algorithms (Taddei et al., 2004). These methods and relationships developed in the field of human and animal biomechanics can also be very valuable to the field of plant biomechanics.

Currently, only a handful of studies have attempted to quantifying the mechanical properties of maize stalk tissues. Longitudinal Young's modulus values were reported to be around 14 GPa (Zhang et al., 2016; Al-Zube et al., 2017, 2018) but a follow-up study reported the modulus of the pith as approximately 0.14 GPa (Zhang et al., 2017). Only one study has reported values for the transverse material properties (Stubbs and Sun et al., 2019). In that study, inverse finite-element methods were used to obtain the transverse Young's modulus of both rind and pith tissues.

The first aim of this study was to assess the feasibility of using CT data to infer the spatial distribution of the transverse Young's modulus within cross-section of maize stalk specimens. The second aim was to assess the validity of such a mapping relationship through secondary tests to validate the predictive utility of the mapping relationship. To the best of our knowledge, this is the first study to use CT to estimate the spatial distribution of material properties of the maize stalk.

2. Methods

2.1. Compression testing

Commercial hybrid maize stalks were used as test specimens for this study. Stalks were air dried to a stable 10–15% water content (dry basis) prior to testing. Stalks were sectioned into specimens that were approximately 10 mm in length (see Fig. 1). The sectioning length of the specimens was decided by balancing a number of factors: (1) the longer the specimen, the more cross-sectional variation that exists, and the less accurate a 2-dimensional finite element model will be, and (2) the shorter the specimen, the more susceptible it will be to error introduced by non-parallel sectioning cuts (i.e. imperfections in the cut will have a larger impact on the calculations of shorter specimens). A length of 10 mm was chosen to balance these factors, as well as to ensure that full free expansion of the ends was allowed. This free expansion of the ends is critical in maintaining a stalk that is as close as possible to the plane stress assumption of the 2-dimensional finite element model.

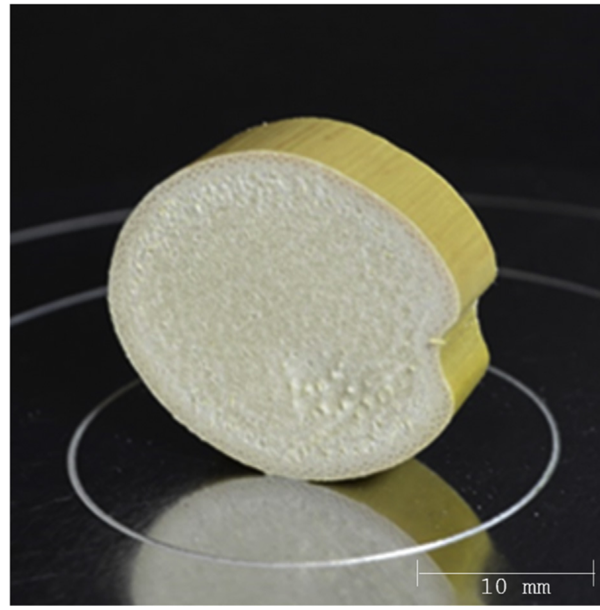

Fig. 1 – A typical compression test specimen (Stubbs and Sun et al., 2019).

Each specimen was tested in transverse compression, loaded through the minor diameter of the specimen cross-section. Next, the pith was removed from each specimen, and they were tested in the same loading configuration. Each test specimen was cut from the stalk using a precision abrasive saw to 10 mm in length. For the solid specimens, an initial load of between 3 N and 10 N was applied to each solid specimen, depending on specimen size. Five loading cycles were then applied. In each loading cycle, the specimen was compressed beyond its pre-loaded state by 0.2 mm, and then the platens were retracted until the initial load was restored. The first four cycles were used as conditioning cycles. Only data from the fifth cycle were employed in the follow-on calculations. For all tests, the displacement rate was 0.05 mm s^{-1} and the sampling frequency was 33 Hz. The testing procedure for hollowed specimens was identical to that of the solid specimens, with the exception that the initial load was reduced to 0.2 N due to the decreased load-bearing capacity of the hollow specimens. Linear force-displacement curves were extracted from each test (Stubbs and Sun et al., 2019). It was found that the rind and pith materials were linearly elastic in the transverse direction. This agrees with previously published data on the linear elastic nature of the rind and pith materials in the longitudinal direction (Al-Zube et al., 2018).

2.2. Finite element model development

The commercial hybrid maize stalks were scanned using an X5000 scanner (NorthStar Imaging, Rogers, MN, USA) at a resolution of 90 μm $voxel^{-1}$. A customised computer program was used to extract the cross-sectional area of each stalk from the CT data (Al-Zube et al., 2017). The extracted morphology was then used to develop a finite element model to simulate the testing in Abaqus/CAE 2016 (Dassault Systèmes, Vélizy-Villacoublay, France). The geometry for the model was created using the inner and outer boundaries derived from the specimen-specific CT scans. The model was designed as a two-dimensional plane-stress analysis. The rind and pith material was found to be transversely isotropic (Stubbs and Sun et al., 2019), and as such were modelled with transversely isotropic material properties. The model was meshed using 4-noded bilinear plane stress quadrilateral elements (Hibbitt et al., 2016; Simulia, 2016). For the analyses that simulated the hollow specimen test configuration, the pith elements were removed.

The finite element models (FEMs) were solved using a non-linear, full Newton direct solver in Abaqus/Standard 2016. The contact between the platens and the specimen was represented by a general contact interaction with a finite-sliding formulation and a hard penalty pressure-overclosure relationship. Tangential friction was used to aid in convergence with a negligibly small coefficient of friction.

2.3. CT mapping of material properties

A mapping equation was required to relate CT data to the finite-element model. The CT scan data consisted of a 3-dimensional array of x-coordinate, y-coordinate, and an 8-bit greyscale value representing the CT intensity of the pixel. A linear relationship between CT intensity and modulus was assumed. The Young's modulus values were mapped to the FEM using a analytical predefined field. Mesh convergence studies were performed to ensure an adequate number of Gauss integration points. It should be noted that the resolution of the model was bounded by the CT scan resolution (90 μm voxel^{-1}). Figure 2 depicts the original CT scan data and the inferred Young's modulus data. It should be noted that Fig. 2 depicts a mesh density of 90 90 μm per element side, which is the same as the CT scan resolution, to depict the relative scale of the voxel resolution to the tissue heterogeneity. Two Poisson's ratios were considered in these analyses. The Poisson's ratio relating the strain in the transverse direction (i.e. the plane of the test) and the longitudinal direction (along the stalk fibre lengths), υ', was considered. As minimal friction between the specimen and the test platens allowed for free expansion of the specimen in the longitudinal direction, the model was analysed an assumption of plane stress. Next, the Poisson's ratio relating the strain in the vertical (loading axis) and horizontal (perpendicular to the loading axis), υ, was considered. Preliminary parametric analyses found that the value of υ within the non-incompressible range ($0 \le \upsilon \le 0.5$) had a negligible effect on the analyses. This is consistent with similar analyses performed previously in our laboratory (Stubbs and Sun et al., 2019). Thus, the Poisson's ratio was set to a value of 0.25 for all analyses. An overview of the mapping process is shown in Fig. 3.

A mapping equation that relates CT intensity (x) with Young's modulus was defined by a linear function with a slope S. In addition, there exists a lower bound CT intensity value (*CT_min*) at which the Young's modulus is 0. Naturally, to prevent non-physical behaviour, all CT intensity values less than this value would also correspond to a Young's modulus of 0. Thus, this relationship can be written in the form:

$$Young's\ Modulus = \left\{ \begin{array}{ll} (x - CT\_min) \cdot S; & x > CT\_min \\ 0; & x \le CT\_min \end{array} \right\} \quad (1)$$

As there exist two unknowns in this function (i.e. S, *CT_min*), a stalk of two analyses to was needed to simultaneously solve to determine these values. These two analyses correspond to the two tests performed on each specimen. In short, determining the CT mapping function was done by solving for the coefficients of Eq. (1) that is capable of accurately reproducing the structural response of both physical tests of a given specimen.

To solve for the coefficients (S and *CT_min*), the following procedure was used: (1) three initial estimates were made of *CT_min* values for each of the two specimen tests, (2) the three corresponding S values were iteratively solved for in each of the two specimen tests, (3) quadratic approximations were found for the two S vs. *CT_min* curves, (4) an estimate was made of the *CT_min* that would result in both analyses having the same S values (the point at which the two curves intersect), (5) the two analysis were both iterated upon at this newly predicted *CT_min* value, and the resulting S values were compared. If the two S values were found to be within 1% of each other, the mapping equation was considered to be valid. Otherwise, steps 2 through 4 were repeated. Graphical representations of this process are shown in Fig. 4.

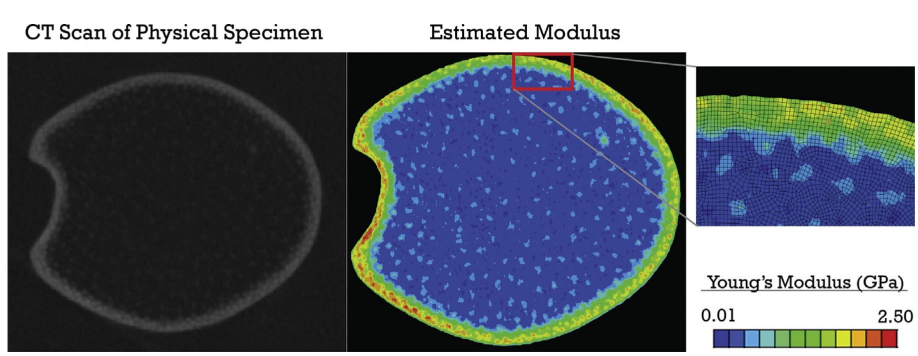

Fig. 2 – Left: A representative CT scan of a single specimen. Right: the corresponding finite element model, mesh, and (in color) the inferred CT intensity values of each element.

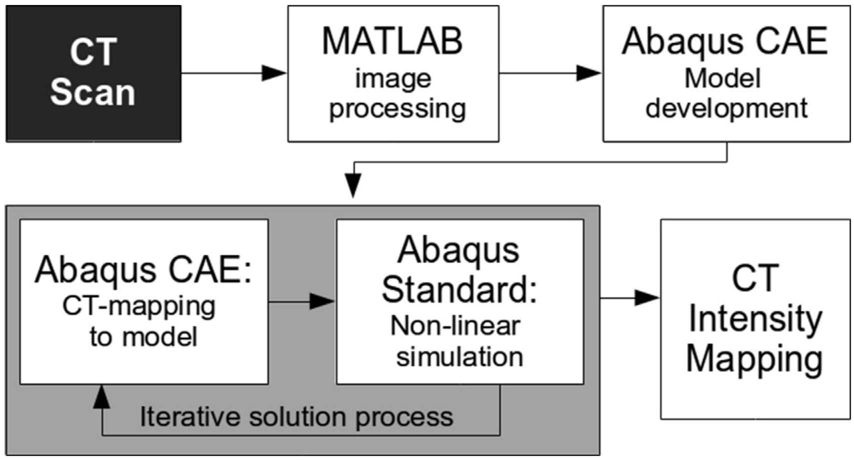

Fig. 3 – The process map for the mapping and validation process.

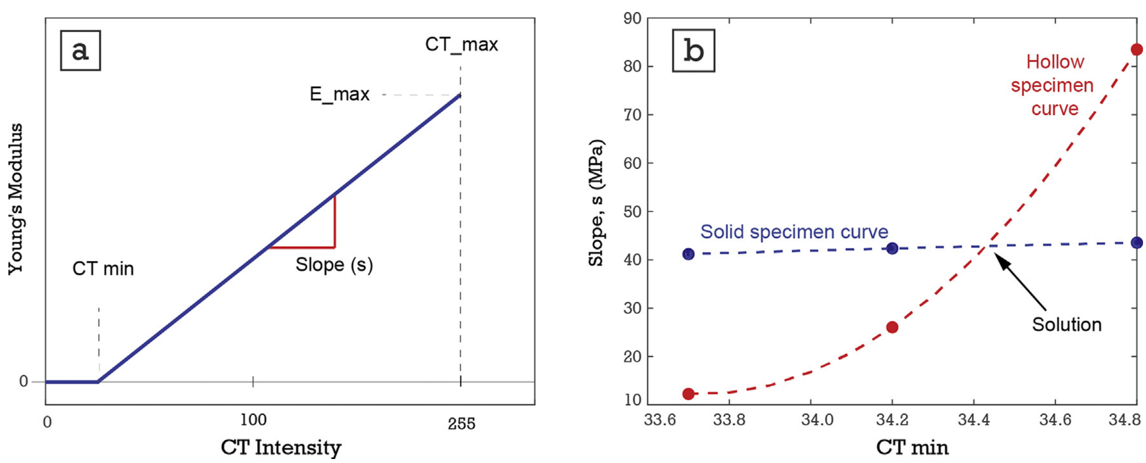

Fig. 4 – Left: The mapping function relating CT intensity to Young's modulus, including the two unknown values CT_min and slope, and the range of CT intensity values found in a typical CT scan of a maize stalk specimen. Right: an example of the valid CT_min and slope pairs for a specimen (right). Quadratic approximations for the two curves were found and iterated to find the intersection of the curves, i.e. the CT_min and s pair that resulted in a CT intensity mapping equation that was valid for both test configurations.

2.4. *Validation*

Mapping relationships were validated using a completely independent data set. This independent validation was performed on the same specimen, providing true independent, paired validation of the approach (Nelson et al., 2019). This was accomplished by testing each specimen in a different orientation: with the compressive load applied along the major axis of the cross-section, as shown in Fig. 5. As the validation testing was performed with the pith intact, these tests were performed prior to the pith removal described in the previous sections. A new FEM was built to simulate this loading configuration, and the CT-mapping equation was applied to the model. The predicted force-displacement structural response of the model was then compared to the force-displacement slope from the physical test.

3. Results

3.1. *Mapping coefficients*

Mapping coefficients were successfully determined using the approach described above. The coefficients of each sample's mapping functions are plotted in Fig. 6, with *CT_min* values along the horizontal axis and slope values along the vertical axis. In this chart, specimens from the same maize stalk are plotted using the same type of symbol (e.g. circle, x).

The elastic moduli values were successfully mapped onto the specimens. Figure 7a depicts a typical specimen with mapped moduli values. Figure 7b depicts a histogram of a typical specimen's mapped elastic moduli values. The mapping clearly depicts the pith, vascular bundles and transition region between rind and pith, and rind tissues as all having differing moduli values. Specifically, it was found that the softest tissue

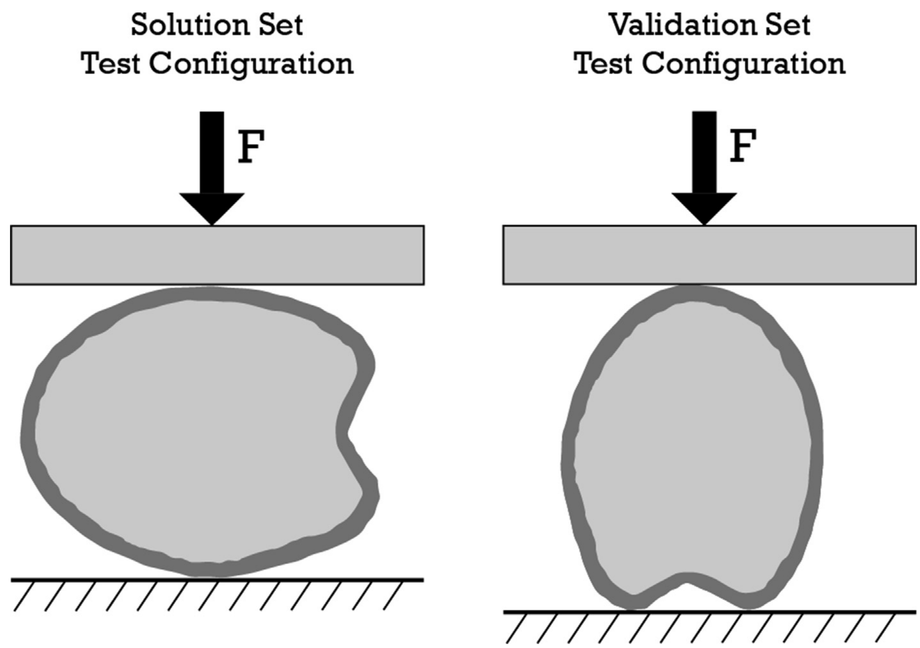

Fig. 5 – The solution set testing configuration (left) and validation testing configuration (right) (Stubbs and Sun et al., 2019).

was the pith (predominately parenchyma) and the stiffest tissue was the rind (predominately sclerenchyma) (Chesson et al., 1997). The vascular bundles were found to be of a stiffness between the rind and pith tissues. These measured values for transverse moduli of the rind and pith are consistent with reported values in the literature for similar materials such as wood (Green et al., 1999; Lakkad & Patel, 1981), as well as previously reported transverse moduli values for maize rind and pith moduli. The average transverse moduli for the pith in Fig. 7b was found to be 0.016 GPa, as compared to 0.026 GPa reported out previously (Stubbs and Sun et al., 2019), and the average transverse moduli for the rind was found to be 1.47 GPa as compared to 0.85 GPa reported previously (Stubbs and Sun et al., 2019).

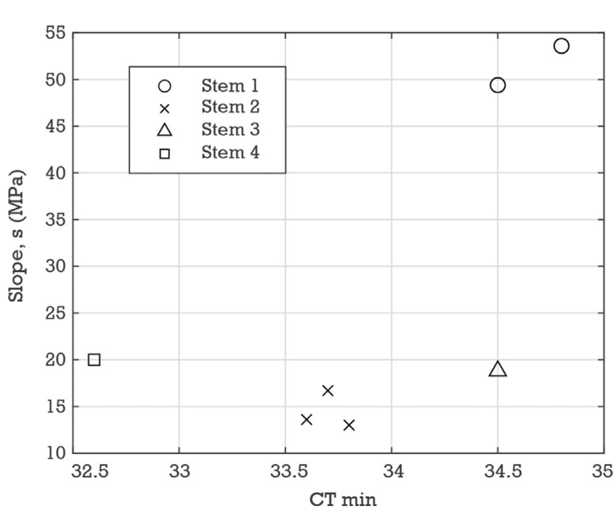

Fig. 6 – The *CT_min* and slope values of the mapping functions of the specimens.

While the *CT_min* coefficient values were quite consistent (coefficient of variation of 2.2%), there was a much higher variation in the slope coefficient (coefficient of variation of 65.5%). The large coefficient of variation of the slope is in fact somewhat misleading, and sheds light on the issue of using an indirect parameter. As the slope is derived from the (*CT_min*, 0) point and the (*CT_max*, *E_max*) point, any variation in these values influence the uncertainty of the slope.

3.2. *Independent validation*

The method for obtaining CT-mapping coefficients ensured that, for each specimen, the modelled vs. measured structural response of solid and hollow specimens were both within 1%. This itself could be considered as a form of validation since a single mapping relationship could be used to accurately predict the response of the specimen in two different configurations (solid and hollow). However, the validity of the mapping relationships and their predictive utility was tested using secondary tests. This was done by creating models of the validation tests in which the load was applied along the major axis of the cross-section (Fig. 5). These models were created by taking the already-analysed models and orienting them to match the validation test, as shown in Fig. 5. It should be noted that these models used the original test data, and they did not consider the repeatability of the compression test. The repeatability and reliability of the compression test protocol was analysed as part of a previous study from our laboratory and determined to be highly repeatable and reliable (Stubbs and Sun et al., 2019).

The comparison between measured and predicted structural responses of each validation model is plotted in Fig. 8. As shown in that figure, the regression line of best fit was very close to the expected 1:1 line. Validation models predicted the

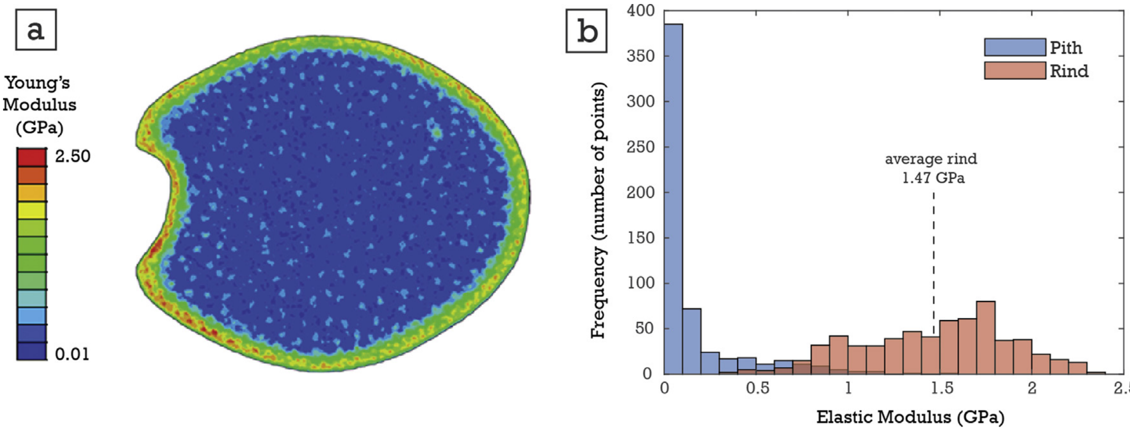

Fig. 7 – The mapping of elastic modulus on the finite element model of a typical specimen (a); the distribution of elastic moduli values in the finite element model (b).

structural response of specimen tests with an average error of 11% (solid models/specimens) and 25% (hollow models/specimens). Thus, the overall average error between predicted and measured was 17%. The ability of the validation models to predict the force-displacement response of the specimen in a different test configuration was considered to be positive validation of the CT-mapping method.

4. Discussion

4.1. *Predictive accuracy*

This study represents the first attempt to obtain CT-mapping relationships for maize tissues. The approach used in this study produced a single pair of CT-mapping coefficients from each specimen. This approach was used because (a) it was anticipated that mapping coefficients would be relatively similar across specimens, and (b) because it provides a very simple and straightforward solution process that minimises

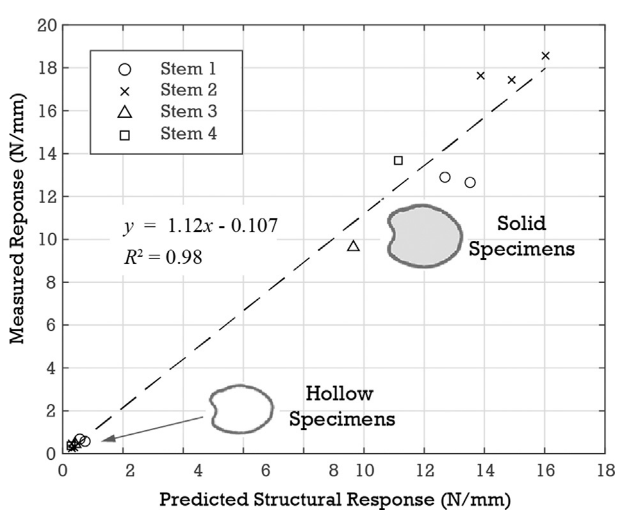

Fig. 8 – The predicted vs. actual structural response of the validation models.

the number of finite-element solutions required to obtain the mapping coefficients. This specimen-specific mapping relationship was used to predict the solid and hollow responses of each individual test specimen, was found to exhibit a reasonable level of error when each specimen is tested in a different configuration.

4.2. *Consistency of mapping coefficients*

While these results are encouraging, the current method is not yet perfected. In this study, all specimens were scanned simultaneously to eliminate the influence of variation within the scanning process itself. It was anticipated that this would provide relatively high consistency between the mapping functions of each specimen. As noted in the results section and shown in Fig. 6, all intercept coefficient (CT_min) values were within 4% of the average. Furthermore, for stalks with multiple specimens (stalks 1 and 2), the CT_min values were within 1% of the average for each group. While CT_min values were highly consistent, the slope coefficients exhibited a much wider level of variation than expected. Higher consistency was observed for specimens from the same stalk (see the data clusters for stalk 1 and stalk 2 in Fig. 6). But even within these groups the variation was several times higher than for CT_min.

The variation in slope is not yet well understood since this study was designed only to test the validity of the approach in general, not to investigate specific sources of variation. Nevertheless several possibilities are suggested by the broader literature. First, it is know from literature concerning wood that X-ray attenuation of dry wood is closely related to its mass density (Freyburger et al., 2009). However, the density/attenuation relationship is also dependent upon other factors such as water content (Lindgren, 1991), wood type (Bergsten et al., 2001), chemical content and X-ray beam energy (Wei et al., 2011). Thus, although density is the *primary* factor associated with X-ray attenuation, many other factors can affect the relationship between density and attenuation. Secondly, while the wood stiffness is also dependent upon mass density (Niklas & Spatz, 2010), the microfibril angle is well-known to have a significant influence on mechanical tissue properties (Downes et al., 2002; Lachenbruch et al., 2010).

Thus, the information from the wood literature suggests that the relationship between CT data and mechanical tissue properties in maize specimens may be influenced by factors that were not measured in this study such as water content, chemical content, microfibril angle, etc. Further research will be required to elucidate these relationships. But based on the positive results from this study as well as the progress made in this area in wood science, it seems highly probably that the mapping relationship between CT data and mechanical properties of maize tissues could be significantly improved with further research.

4.3. Stalk lodging

The ultimate purpose of this work is to help researchers better understand the stress fields within plant specimens under external loads. It has been shown that during late season lodging of maize specimens, the materials are low in moisture and are senescing (similar to the testing configuration presented herein), and failure occurs at low displacements with a brittle material response (Barnwal et al., 2012; Cook et al., 2019; Stubbs and Oduntan et al., 2020). As such, linear material properties and small strain material behaviour are relevant to modelling the failure of late season maize stalks. These stalks typically lodge due to tissue or buckling failure at random heights along the stalk (Stubbs and Larson et al., 2019; Stubbs and Seegmiller et al., 2020). Although buckling failure is not necessarily dependent on the stress field of the stalk, tissue failure certainly is. However, further work is still required to fully quantify the extent of nonlinearity in the material prior to tissue failure.

4.4. Limitations

This study was conducted to determine the feasibility of using CT intensity data to infer spatial variations of the transverse Young's modulus on a per-specimen basis. The results suggest that this approach is possible and that future research will likely lead to refined mapping relationships. However, this preliminary attempt is not without limitations, which are discussed in this section.

Firstly, CT-scanning is typically only feasible using dried specimens because water tends to absorb much more X-ray radiation than the dry matter of a stalk. This not a serious limitation in the study of maize stalks since the failure of maize stalks just before harvest is of interest and this is when they are relatively dry. However, this method may not be suitable for inferring the mechanical properties of wet stalks. Secondly, in this study a linear relationship between CT intensity and material stiffness is assumed. While the density-stiffness relationship of cellular materials is well-established (Gibson, 2005), X-ray absorption is a relatively complex phenomenon which is likely not to be linear in nature. Thus, a non-linear approximation may provide a more accurate approximation of the behaviour of the structure.

Thirdly, the validation approach used in this study relied upon overall structural responses rather than the direct measurement of material properties. The close agreement found between predicted and measured responses is certainly encouraging, and is likely to be correct. However, the mapping relationship itself was not tested directly. The authors have previously considered the use of indentation techniques to assess the local longitudinal stiffness of maize tissues, but at the microscale, maize tissue is highly inhomogeneous. This makes such approaches very difficult. As more sophisticated material assessment techniques become available, it may be possible to more directly assess the accuracy of CT/tissue mapping relationships. Fourthly, only a single transverse CT scan layer was used for each specimen and the finite-element model was two-dimensional. This approach ignores any changes in the transverse cross-section along the length of the specimen. Further improvements to the method could be obtained through taking into account changes in the cross-section and the spatial distribution of tissue stiffness along the length of the specimens. Finally, the solution approach used in this study provided specimen-specific coefficient pairs instead of a single pair of coefficients that was simultaneously optimised across the entire set of specimens.

5. Conclusions

A method was developed for inferring the spatial distribution of the transverse Young's modulus within cross-section of maize stalk specimens form CT scan data. The method exhibited very low errors on a per-specimen basis under initial loading conditions, and when these same specimens were tested in secondary configurations, the CT-informed material mapping was able to predict specimen behaviour with an average error of 17%. These results indicate that CT scan data can be used to infer the spatial distribution of transverse Young's modulus within plant specimens, an approach which will enable more detailed studies that consider material heterogeneity.

This approach provides researchers with the tools required to develop a better mechanistic understanding of the stress fields within a plant stalk during external loading. This is important for two reasons: (1) it provides researchers with a better understanding of how stresses are developed through and between the tissue types, and (2) this represents an essential step in the development of a multiscale computational modelling framework for the structural tissue of plant stalks.

Availability of data and materials

The datasets used and/or analysed during the current study are available from the corresponding author on reasonable request.

Declaration of competing interest

The authors declare that they have no known competing financial interests or personal relationships that could have appeared to influence the work reported in this paper.

Acknowledgements

This work was funded in part by Bayer Crop Science (St. Louis, MO 63141, formerly Monsanto Company) and the National Science Foundation, USA (Award # 1400973). We thank Bayer Crop Science for providing the maize stalk samples used in this study.

REFERENCES

Al-Zube, L. A., Robertson, D. J., Edwards, J. N., Sun, W. H., & Cook, D. D. (2017). Measuring the compressive modulus of elasticity of pith-filled plant stems. *Plant Methods, 13*. https://doi.org/10.1186/s13007-017-0250-y

Al-Zube, L., Sun, W., Robertson, D., & Cook, D. (2018). The elastic modulus for maize stems. *Plant Methods, 14*(1), 11. https://doi.org/10.1186/s13007-018-0279-6

Barnwal, P., Kadam, D., & Singh, K. (2012). Influence of moisture content on physical properties of maize. *International Agrophysics, 26*(3), 331. https://doi.org/10.2478/v10247-012-0046-2

Bergsten, U., Lindeberg, J., Rindby, A., & Evans, R. (2001). Batch measurements of wood density on intact or prepared drill cores using x-ray microdensitometry. *Wood Science and Technology, 35*(5), 435–452. https://doi.org/10.1007/s002260100106

Chesson, A., Provan, G. J., Russell, W., Scobbie, L., Chabbert, B., & Monties, B. (1997). Characterisation of lignin from parenchyma and sclerenchyma cell walls of the maize internode. *Journal of the Science of Food and Agriculture, 73*(1), 10–16. https://doi.org/10.1002/(SICI)1097-0010(199701)73:1<10::AID-JSFA697>3.0.CO;2-E

Ciarelli, M. J., Goldstein, S. A., Kuhn, J. L., Cody, D. D., & Brown, M. B. (1991). Evaluation of orthogonal mechanical properties and density of human trabecular bone from the major metaphyseal regions with materials testing and computed tomography. *Journal of Orthopaedic Research, 9*(5), 674–682.

Cook, D. D., de la Chapelle, W., Lin, T. C., Lee, S. Y., Sun, W., & Robertson, D. J. (2019). Darling: A device for assessing resistance to lodging in grain crops. *Plant Methods, 15*(1), 102. https://doi.org/10.1186/s13007-019-0488-7

Cuy, J. L., Mann, A. B., Livi, K. J., Teaford, M. F., & Weihs, T. P. (2002). Nanoindentation mapping of the mechanical properties of human molar tooth enamel. *Archives of Oral Biology, 47*(4), 281–291.

Downes, G. M., Nyakuengama, J. G., Evans, R., Northway, R., Blakemore, P., Dickson, R. L., & Lausberg, M. (2002). Relationship between wood density, microfibril angle and stiffness in thinned and fertilized Pinus radiata. *International Association of Wood Anatomists Journal, 23*(3), 253–265. https://doi.org/10.1163/22941932-90000302

Freyburger, C., Longuetaud, F., Mothe, F., Constant, T., & Leban, J. M. (2009). Measuring wood density by means of X-ray computer tomography. *Annals of Forest Science, 66*(8), 804. https://doi.org/10.1051/forest/2009071

Gibson, L. J. (2005). Biomechanics of cellular solids. *Journal of Biomechanics, 38*, 377–399. https://doi.org/10.1016/j.jbiomech.2004.09.027

Gourion-Arsiquaud, S., Burket, J. C., Havill, L. M., DiCarlo, E., Doty, S. B., Mendelsohn, R., van der Meulen, M. C., & Boskey, A. L. (2009). Spatial variation in osteonal bone properties relative to tissue and animal age. *Journal of Bone and Mineral Research, 24*, 1271–1281. https://doi.org/10.1359/jbmr.090201

Green, D. W., Winandy, J. E., & Kretschmann, D. E. (1999). Mechanical properties of wood. *Wood handbook: wood as an engineering material* (pp. 4.1–4.45, 113). Madison, WI: USDA Forest Service, Forest Products Laboratory. General technical report FPL; GTR-113.

Hammond, M. A., Wallace, J. M., Allen, M. R., & Siegmund, T. (2018). Incorporating tissue anisotropy and heterogeneity in finite element models of trabecular bone altered predicted local stress distributions. *Biomechanics and Modeling in Mechanobiology, 17*, 605–614. https://doi.org/10.1016/0021-9290(84)90029-0

Helgason, B., Taddei, F., Pálsson, H., Schileo, E., Cristofolini, L., Viceconti, M., & Brynjólfsson, S. (2008). A modified method for assigning material properties to FE models of bones. *Medical Engineering & Physics, 30*, 444–453. https://doi.org/10.1016/j.medengphy.2007.05.006

Hibbitt, K., Karlsson, B. I., & Sorenson, E. P. (2016). *ABAQUS/Standard theory manual*. Sorenson Inc.

Kaneko, T. S., Bell, J. S., Pejcic, M. R., Tehranzadeh, J., & Keyak, J. H. (2004). Mechanical properties, density and quantitative CT scan data of trabecular bone with and without metastases. *Journal of Biomechanics, 37*(4), 523–530. https://doi.org/10.1016/j.jbiomech.2003.08.010

Kaneko, T. S., Pejcic, M. R., Tehranzadeh, J., & Keyak, J. H. (2003). Relationships between material properties and CT scan data of cortical bone with and without metastatic lesions. *Medical Engineering & Physics, 25*(6), 445–454. https://doi.org/10.1016/S1350-4533(03)00030-4

Lachenbruch, B., Johnson, G. R., Downes, G. M., & Evans, R. (2010). Relationships of density, microfibril angle, and sound velocity with stiffness and strength in mature wood of Douglas-fir. *Canadian Journal of Forest Research, 40*(1), 55–64. https://doi.org/10.1139/X09-174

Lakkad, S. C., & Patel, J. M. (1981). Mechanical properties of bamboo, a natural composite. *Fibre Science and Technology, 14*(4), 319–322.

Lindgren, L. O. (1991). Medical CAT-scanning: X-Ray absorption coefficients, CT-numbers and their relation to wood density. *Wood Science and Technology, 25*(5), 341–349. https://doi.org/10.1007/BF00226173

Liu, C., Cabahug-Zuckerman, P., Stubbs, C., Pendola, M., Cai, C., Mann, K. A., & Castillo, A. B. (2019). Mechanical loading promotes the expansion of primitive osteoprogenitors and organizes matrix and vascular morphology in long bone defects. *Journal of Bone and Mineral Research, 34*(5), 896–910.

Manjubala, I., Liu, Y., Epari, D. R., Roschger, P., Schell, H., Fratzl, P., & Duda, G. N. (2009). Spatial and temporal variations of mechanical properties and mineral content of the external callus during bone healing. *Bone, 45*, 185–192. https://doi.org/10.1016/j.bone.2009.04.249

McBroom, R. J., Hayes, W. C., Edwards, W. T., Goldberg, R. P., & White, A. A. D. (1985). Prediction of vertebral body compressive fracture using quantitative computed tomography. *Journal of Bone and Joint Surgery, 67*(8), 1206–1214.

Nelson, N., Stubbs, C. J., Larson, R., & Cook, D. D. (2019). Measurement accuracy and uncertainty in plant biomechanics. *Journal of Experimental Botany, 70*(14), 3649–3658. https://doi.org/10.1093/jxb/erz279

Niklas, K. J., & Spatz, H. C. (2010). Worldwide correlations of mechanical properties and green wood density. *American Journal of Botany, 97*(10), 1587–1594. https://doi.org/10.3732/ajb.1000150

Rho, J. Y., Hobatho, M. C., & Ashman, R. B. (1995). Relations of mechanical properties to density and CT numbers in human bone. *Medical Engineering & Physics, 17*(5), 347–355.

Simulia, D. S. (2016). *ABAQUS analysis manual* (Providence, RI, USA).

Snyder, S. M., & Schneider, E. (1991). Estimation of mechanical properties of cortical bone by computed tomography. *Journal of*

Orthopaedic Research, 9(3), 422–431. https://doi.org/10.1002/jor.1100090315
Stubbs, C. J., Larson, R., & Cook, D. D. (2019a). Maize stem buckling failure is dominated by morphological factors. *BioRxiv*, 833863. https://doi.org/10.1101/833863
Stubbs, C. J., Seegmiller, K., McMahan, C., Sekhon, R. S., & Robertson, D. J. (2020a). Diverse maize hybrids are structurally inefficient at resisting wind induced bending forces that cause stalk lodging. *Plant Methods, 16*, 1–15. https://doi.org/10.1101/2020.01.21.914804
Stubbs, C. J., Sun, W., & Cook, D. D. (2019). Measuring the transverse Young's modulus of maize rind and pith tissues. *Journal of Biomechanics, 84*, 113–120. https://doi.org/10.1016/j.jbiomech.2018.12.028
Stubbs, C. J., Oduntan, Y. A., Keep, T. R., Noble, S. D., & Robertson, D. J. (2020). 2020. The effect of plant weight on estimations of stalk lodging resistance. *Plant methods, 16*(1), 1–18.
Teo, J. C., Si-Hoe, K. M., Keh, J. E., & Teoh, S. H. (2006). Relationship between CT intensity, micro-architecture and mechanical properties of porcine vertebral cancellous bone. *Clinical Biomechanics, 21*(3), 235–244. https://doi.org/10.1016/j.clinbiomech.2005.11.001
Wei, Q., Leblon, B., & La Rocque, A. (2011). On the use of X-ray computed tomography for determining wood properties: A review. *Canadian Journal of Forest Research, 41*(11), 2120–2140. https://doi.org/10.1139/x11-111
Wimmer, R., Lucas, B. N., Oliver, W. C., & Tsui, T. Y. (1997). Longitudinal hardness and Young's modulus of spruce tracheid secondary walls using nanoindentation technique. *Wood Science and Technology, 31*, 131–141. https://doi.org/10.1007/BF00705928
Zhang, J., Yan, C. H., Chui, C. K., & Ong, S. H. (2010). Accurate measurement of bone mineral density using clinical CT imaging with single energy beam spectral intensity correction. *IEEE Transactions on Medical Imaging, 29*(7), 1382–1389. https://doi.org/10.1109/TMI.2010.2045767
Zhang, L., Yang, Z., Zhang, Q., & Guo, H. (2016). Tensile properties of maize stalk rind. *BioResources, 11*(3), 6151–6161. https://doi.org/10.1520/A0370-14
Zysset, P. K., Guo, X. E., Hoffler, C. E., Moore, K. E., & Goldstein, S. A. (1999). Elastic modulus and hardness of cortical and trabecular bone lamellae measured by nanoindentation in the human femur. *Journal of Biomechanics, 32*(10), 1005–1012.

Glossary

CT: an abbreviation for x-ray computed tomography
Lodging: the failure of the maize stalk due to wind-induced bending loads
Pith: soft, spongy tissue in the center of the stems of vascular plants
Rind: the tough outer layer in the stems of vascular plants
Stalk: in maize, the main structural axis of the plant, excluding leaves and reproductive organs
Vascular bundle: a structure in maize primarily responsible for fluid transport

Symbols

x: a variable representing CT intensity
CT_min: the value of x at which the Young's modulus is set to 0
E: Young's modulus
E_max: the Young's modulus value corresponding to *CT_max*
S: the slope of the mapping from CT intensity to Young's modulus
CT_max: the maximum possible value of x based on CT data. In this study, $CT\_max = 255$